Femto to microsecond dynamics of excited electrons in a quadruple cation perovskite

Eunhwan Jung[a†], Kestutis Budzinauskas[b†], Senol Öz[a,c†], Feray Ünlü[a], Henning Kuhn[b], Julian Wagner[b], David Grabowski[d], Benjamin Klingebiel[d], Marie Cherasse[e], Jingwei Dong[e], Pierfrancesco Aversa[e], Paola Vivo[f], Thomas Kirchartz[d,g], Tsutomu Miyasaka[c], Paul H. M. van Loosdrecht[b], Luca Perfetti[e*] and Sanjay Mathur[a*]*

a Institute of Inorganic Chemistry, University of Cologne, Greinstr. 6, 50939, Cologne, Germany

b Institute of Physics 2, University of Cologne, Zülpicher str. 77, 50937, Cologne, Germany

c Graduate School of Engineering, Toin University of Yokohama, 1614 Kuroganecho, Aoba, Yokohama, Kanagawa 225-8503, Japan

d IEK-5 Photovoltaik, Forschungszentrum Jülich GmbH, 52425 Jülich, Germany

e Laboratoire des Solides Irradiés, Ecole Polytechnique, CNRS, CEA/DRF/IRAMIS,Institut Polytechnique de Paris, 91128 Palaiseau Cedex, France

f Faculty of Engineering and Natural Sciences, Tampere University,P.O. Box 541, FI-33101 Tampere, Finland

g Faculty of Engineering and CENIDE, University of Duisburg-Essen, Carl-Benz-Str. 199, 47057 Duisburg, Germany

AUTHOR INFORMATION

Corresponding Author

*Sanjay.Mathur@uni-koeln.de

*(co corresponding) luca.perfetti@polytechnique.edu

*(co corresponding) pvl@ph2.uni-koeln.de

Abstract

Quadruple cation mixed halide perovskite, $GA_{0.015}Cs_{0.046}MA_{0.152}FA_{0.787}Pb(I_{0.815}Br_{0.185})_3$, single crystals were grown for the first time using an inverse temperature crystallization process. Solar cell devices in n-i-p stack configuration using thin films of the same materials showed power conversion efficiency above 20%. Complementary time resolved spectroscopy confirmed that polycrystalline thin films and single crystals identically composed exhibit similar carrier dynamics in picosecond range. Cooling of excited carriers and bandgap renormalization occur on the same timescale of 200 – 300 fs. The radiative recombination rate (1.2×10^{-9} cm^3/s) is comparable to values reported for GaAs semiconductor. At low excitation density, a long carrier lifetime of 3.2 µs was recorded possibly due to the passivation of recombination centers. This study clarifies discrepancies about lifetime of hot carriers, impact of radiative recombination, and role of recombination centers on solar cell performance. The quadruple cation perovskites displayed short time dynamics with slow recombination of charge carriers.

TOC GRAPHICS

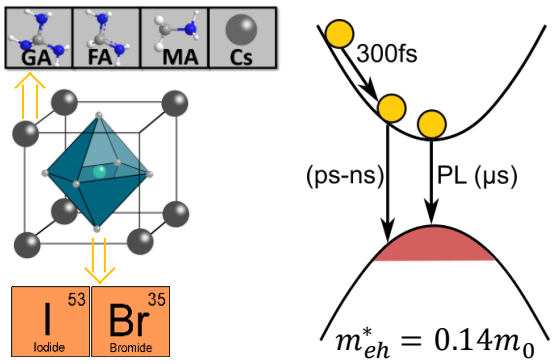

Metal-halide hybrid perovskites represent a family of crystalline compounds that possess crystal structure similar to the parent mineral $CaTiO_3$. These materials can be thus generally described

by the ABX_3 formula, where the A- and B-sites are occupied by monovalent, divalent or tetravalent cations and the X-site is occupied by negatively charged anions. Since their first demonstration in photovoltaic devices ten years ago as solution processed polycrystalline thin films, they have proven to be valuable in a wide range of optoelectronic applications such as light emission, lasing, radiation detection and even as media for energy storage, far beyond the classic solar light harvesting.[1–6] Nonetheless, most of these compounds face inherent as well as externally induced stability issues, which impair and retard their potential commercial applications despite several attempts made to overcome this inherent problem. The most promising results for polycrystalline thin films have been obtained by optimally intermixing different cations on the A-site and halide anions on the X-site of the ABX_3 hybrid perovskite structure. A careful compositional engineering can result in to a cubic phase that: i) is stable within the operation temperature range of a photovoltaic device, ii) maintains a reasonably low band gap value and iii) displays low carrier recombination rates.[7–12] Such an approach allowed the fabrication of small area solar cells having high photoconversion efficiency and stable power output under 1000 hours of 1 sun (100 mW/cm^2) continuous irradiation.[13,14] Most notably, the addition of guanidinium cations could modulate morphology and drastically alter charge recombination dynamics in hybrid perovskites by means of larger grain size, trap passivation and reduced hysteresis effects.[9,10,14,15] Being inspired by recent reports, we have designed and realized a quadruple cation organic-inorganic mixed lead halide perovskite active layer, as well as single crystals, by mixing formamidinium (FA), methylammonium (MA), guanidinium (GA), and cesium (Cs) cations in the desired ratio $GA_{0.015}Cs_{0.046}MA_{0.152}FA_{0.787}Pb(I_{0.815}Br_{0.185})_3$.[8,9,11,16] The photovoltaic performances of GACsMAFA have been tested by fabricating a *n-i-p* type perovskite solar cell architecture with spiro-OMeTAD as the hole transporting material and

compact-TiO_2/mesoporous TiO_2 layer as the electron selective contact. By optimization of the charge extraction at the electron-selective interface, we could achieve a photoconversion efficiency above 20% and negligible hysteresis. Due to the optimal mixing of different cations, the photovoltaic cells displayed a decent operational stability.

It is still an ongoing debate whether the introduction of multiple cations to the perovskite structure could alter the charge carrier dynamics and in particular the effect of trap passivating properties of guanidinium cations are not understood[10,14]. When compared to the previous reports, the main novelty of this work lies in a thorough analysis of the carrier kinetics ranging from femtoseconds to microseconds in multiple cation mixed halide GACsMAFA crystals and films. By applying complementary pump-probe techniques, we prove that an initial photo carrier induced reduction of the optical gap (also known as the band gap renormalization), takes place while carriers are in a highly non equilibrium state. We find no evidence of hot carriers having sizable excess energy and living on picosecond timescale in our quadruple cation samples. This controversial issue has recently been the focus of many experimental studies[17–19] on $CH_3NH_3PbI_3$ and has so far not been addressed in lead halide perovskites with multiple cations. After an ultrafast thermalization, the carriers recombine via radiative pathways at high photoexcitation density or by trap-assisted mechanisms in the low photoexcitation regime. The radiative recombination rate is comparable to the one of standard semiconductors with direct band gap and does not have significant effect in perovskite devices as long as the carrier mobility remains high.[20] In agreement with previous reports,[7–11] we found that inclusions of guanidinium cations in the perovskite mixture passivate the grain boundaries of thin films and increase the non-radiative recombination time up to the microsecond timescale. Finally, the evolution of band filling as a function of photoexcitation density has been employed to estimate the reduced

effective mass near to the band edges. The derived value is comparable[21,22] to the one reported for $CH_3NH_3PbI_3$ and suggests that excited electrons are large polarons with moderate or weak interaction with the lattice polarization.[23]

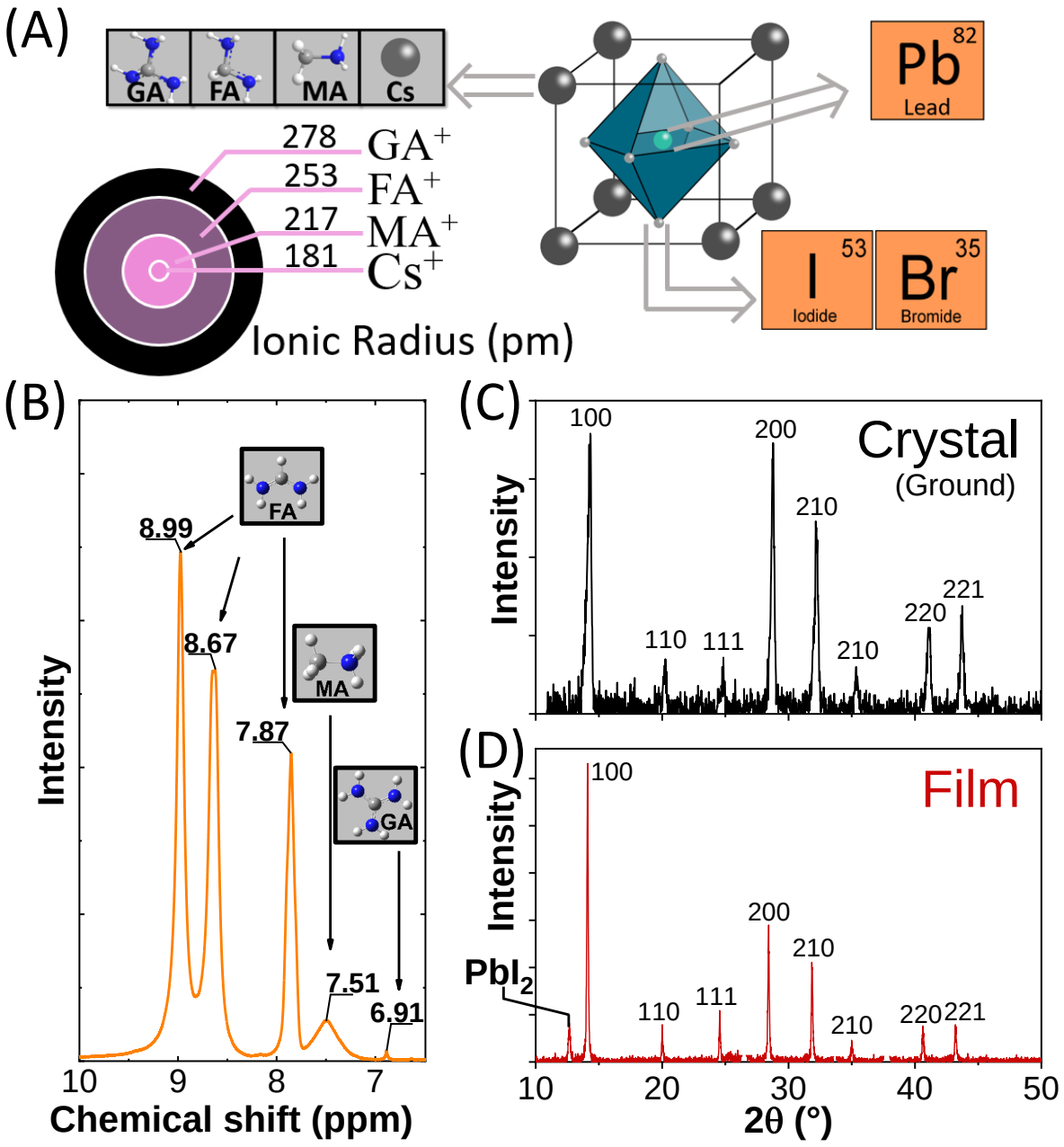

Figure 1. (A) Schematic representation of the unit cell of organic-inorganic ABX_3 perovskite. A = organic or inorganic cations (MA = $(CH_3NH_3^+)$, FA = formamidinium $(HC(NH_2)_2^+)$, GA = guanidinium $(C(NH_2)_3^+)$, Cs^+), B = Pb^{2+} and X = I^-, Br^- and ionic radius of different A-site components. (B) Proton nuclear magnetic resonance (^1H NMR) spectra of single crystals dissolved in DMSO-d_6 show chemical shifts of the hydrogen signal characteristic for each of the

organic cations. (C) Powder X-Ray Diffraction pattern (PXRD) of the $GA_{0.015}Cs_{0.046}MA_{0.152}FA_{0.787}Pb(I_{0.815}Br_{0.185})_3$ ground single crystals. (D) XRD of the $GA_{0.015}Cs_{0.046}MA_{0.152}FA_{0.787}Pb(I_{0.815}Br_{0.185})_3$ thin film. The extra Bragg peak visible around 12.65 degrees is due to excess PbI_2 (5%).

The quadruple cation $GA_{0.015}Cs_{0.046}MA_{0.152}FA_{0.787}Pb(I_{0.815}Br_{0.185})_3$ (GACsMAFA) perovskite (Fig. 1A) has been synthesized as single crystals and as thin films. The synthesis of the single crystals was conducted in nitrogen environment by inverse temperature crystallization (ITC) approach at 107 °C by dissolving the precursor materials in γ-butyrolactone solvent and subsequently performing seed growth under isothermal conditions.[24] Thin films have been prepared via spin coating under nitrogen environment in mixed DMF/DMSO solvent system followed by anti-solvent (toluene) quenching. Each one of the cations covers a functional role in the active layer. The most studied perovskite is based on methylammonium (MA) cation, which is an excellent light harvester but suffers from its low thermal and chemical stability. As an example, direct contact of MA based perovskite with basic metal oxides like ZnO or Cu_2O can lead to deprotonation and subsequent formation of methylamine gas along with other products.[25] Formamidinium (FA) displays a broader absorption of the solar spectrum[26,27] due to its lower band gap and high probability of forming hydrogen bonds.[28] In addition, the FA cation is less prone to deprotonation, when compared to MA, mostly due to the resonance stabilization effects. The optimal embedment of such cation stabilizes the pseudo-cubic or trigonal structure with respect to the tetragonal one that is observed for $MAPbI_3$ under standard conditions. Nonetheless, the $FAPbI_3$ perovskite is also prone to undergo phase transition into the non-photoactive hexagonal δ-phase.[29] This undesirable phase leads to a large bandgap insulator with unsuitable absorption properties for a photoactive layer. However, it is possible to hinder the formation of

the δ-phase by incorporating small amounts of cesium cations as was recently demonstrated by Saliba et al.[29] The latter increases the structural stiffness, suppresses formation of undesired phases, improves thermal stability and distributes the halide mixture evenly throughout the material. Finally, guanidinium (GA) cation suppresses the formation of halide vacancies, and minimizes the non-radiative charge carrier recombination at grain boundaries.[7] GA cation is also very stable since the high pK_a value (13.6) makes any deprotonation process practically impossible. In our study, samples were prepared with 18.5% of bromide and 81.5% of iodide. The chosen bromide and iodide ratio optimizes the optical gap while preserving a cubic structure. The relative concentration of the different cations plays a primary role on the crystal structure as well as on the endurance of the solar cells. We have designed the quadruple cation perovskite in order to achieve the highest possible structural stability. The effective Goldschmidt tolerance factor t_{eff} has been maintained very near to the recommended value for the crystallization in a cubic phase. We obtained $t_{eff} = 0.968$ from an optimal mix of cations in $GA_{0.015}Cs_{0.046}MA_{0.152}FA_{0.787}Pb(I_{0.815}Br_{0.185})_3$.

After synthesis, we have verified the stoichiometry of the compound by performing ^1H Nuclear Magnetic Resonance (NMR) spectroscopy on dissolved single crystals. The single crystal was washed with isopropyl alcohol before dissolve in DMSO-d_6 to ensure removal of surface bound residues. The resonance peaks in the spectrum of Fig. 1B unambiguously identified FA, MA, and GA through the chemical shift of protons belonging to the respective $-NH_2$, $-CH$, $-NH_3^+$ and $-CH_3$ (not shown) groups of the hosting cations. The protons of $-NH_3^+$ (MA) group were observed at 7.51 ppm, while two peaks with identical integral were observed for the $=NH_2^+/-NH_2$ groups of the formamidinium cation at 8.99 and 8.67 ppm, respectively. The double peak structure of the $=NH_2^+/-NH_2$ resonance was only resolvable in a multiple scan NMR spectrum, which enables

a resolution of 0.02ppm (Fig. 1B), whereas in a single scan NMR, the transition is seen at the average position between two peaks (8.99 + 8.67) / 2 = 8.83 as it is shown in the Fig. S3 The -CH group of the FA cation peaked at 7.87 ppm. For the guanidinium cation a single peak at 6.91 ppm was detected, as expected for three chemically equivalent $-NH_2^{1/3+}$ groups. An accurate quantification of the individual components by peak integration indicated an excellent match with the intended composition (see ^{1}H NMR reference spectra Section in the Supporting Informaion).

The phase purity as well as the crystallinity of the compound has been investigated by X-ray diffractometry. The diffraction pattern of single crystal powders in Fig. 1C is compatible with a Pm-3m cubic structure and lattice parameter a = 6.2185 Å (V = 240.4677 Å^3), which were derived from single crystal X-ray diffraction analysis performed using Mo-K_α irradiation. We could not detect any signature of the undesirable δ-phase compound. As shown in Fig. 1D, the X-ray diffraction plot of thin films is nearly identical to the one of the crystalline powders with only notable difference being an extra diffraction peak around 12.65 degrees that is ascribed to excess PbI_2 inclusions. Such minor PbI_2 component has been generated on purpose during the thin film synthesis, by adding an excess quantity of PbI_2. In agreement with previous reports,[32] the enrichment with PbI_2 hinders the accumulation of organic species at the grain boundaries, favors an optimal embedding of the grains and improves the transport of charge carriers.

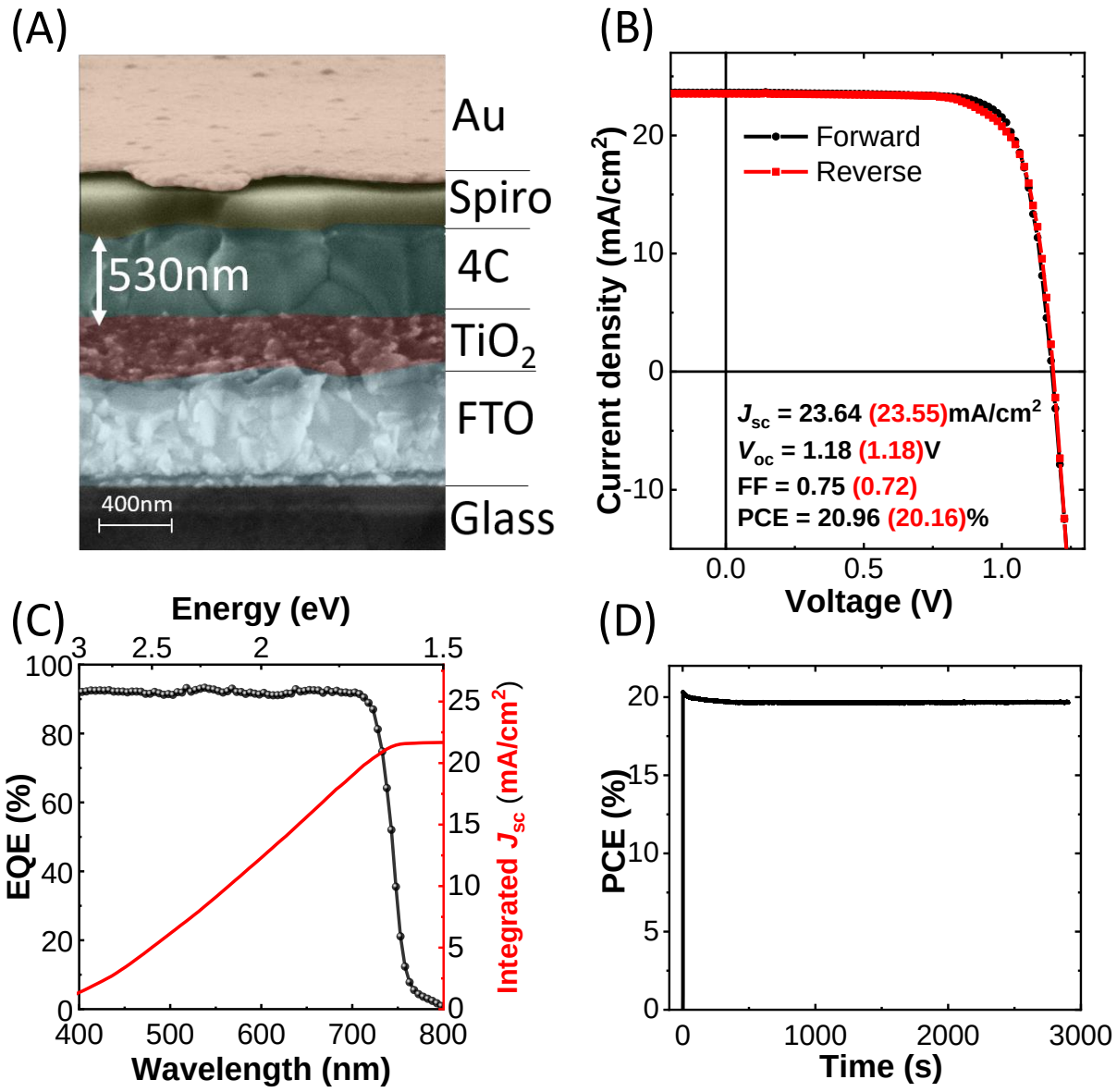

Figure 2. (A) Cross sectional SEM image of a photovoltaic n-i-p device with: 500 nm of transparent electrode FTO, 400 nm of electron transport layer $Li(TFSI)_2$ mp-TiO_2 + perovskite, 530 nm of active perovskite layer $GA_{0.015}Cs_{0.046}MA_{0.152}FA_{0.787}Pb(I_{0.815}Br_{0.185})_3$ and 280 nm of the hole transport layer Spiro-OMeTAD. (B) J-V curve of the device showing: short circuit current density of 23.6 mA/cm^2, open circuit voltage of 1.18 V and an average power conversion efficiency (PCE) of 20.5%. (C) External Quantum Efficiency (EQE) as a function of the incident

photon energy. (D) Maximum Power Point (MPP) tracking during the first hour under illumination AM1.5G 100 mW/cm^2.

A mesoporous-TiO_2 supported architecture was used for the assembly of solar cell devices. The cross-sectional SEM of the regular n-i-p device stack are shown in Fig. 2A. A compact TiO_2 layer was prepared by aerosol spray-pyrolysis on fluorine doped tin oxide (FTO) substrates. A mesoporous TiO_2 layer has been deposited by spin coating and treated with Li-TSFI according to Saliba and Giordano et al.[29,33] The thermally induced decomposition of the Bis(trifluoromethane)sulfonamide anion (TFSI) in the presence of alkali elements passivates the surface of TiO_2 via Ti-O-S-O-Pb bridges, while lithium effectively modulates the electronic conductivity and reduces the non-radiative recombination centers related to oxygen vacancies.[34] The GACsFAMA film was deposited on Li-doped mesoporous TiO_2. Finally, the perovskite GACsFAMA film was capped by a spiro-OMeTAD layer and a thermally evaporated gold cathode. Within this n-i-p architecture, the TiO_2 material acts as the electron selective transport layer (ETM), while the spiro-OMeTAD selectively extracts and transports the holes (HTM) towards the gold contact. The thin film SEM cross section displayed (Fig. 2A) homogeneous filling and good contact quality. The J-V curve in Fig. 2B resulted in a power conversion efficiency (PCE) of 20.96% in the forward direction and 20.12% in the reverse direction. We have measured the power density output with 1 sun of illumination on a device of 0.16 cm^2. As shown by Fig. 2C, a stable photocurrent power output of about 19.5 mW/cm^2 (PCE of 20.5 %), stabilized within a few seconds and remained constant throughout the entire duration of the measurement. We emphasize that the J-V hysteresis in Fig. 2B is remarkably low compared to other solar cells fabricated using TiO_2 and Spiro-OMeTAD as transport layers[35] or GACsMAFA as absorber.[8,9,36] This finding is ascribed to several factors: i) Guanidinium, due to its hydrogen

bonding capability, enhances grain size and passivates under-coordinated iodide species between adjacent crystalline grains. ii) GA and the excess PbI_2 minimize the halide ions migration at the interface[7] iii) lithium incorporation in mesoporous TiO_2 reduces the oxygen vacancies, iv) the smooth roughness of the thin film, observed with AFM measurements (Fig. S2C), allows for a good charge extraction and hinders the formation of volatile capacitances.[36] As shown in Fig. 2C, the External Quantum Efficiency (EQE) of our *n-i-p* architecture is larger than 80% in the entire range covered by the visible light. This observation confirms that most of the photo-generated electrons and holes can be collected before recombination, despite the relatively high thickness of the active layer of almost 1 μm (400 nm perovskite/mp-TiO_2 and 530 nm perovskite capping layer). This could be explained by good carrier transport properties, confirmed by a diffusion coefficient of 0.05 cm^2s^{-1} for GACsFAMA film which was measured with a non-invasive transient grating method (Fig. S5). This value fits well with a typical diffusion coefficient found in other halide perovskites varying from 0.01 cm^2s^{-1} to 0.18 cm^2s^{-1}.[37,38]

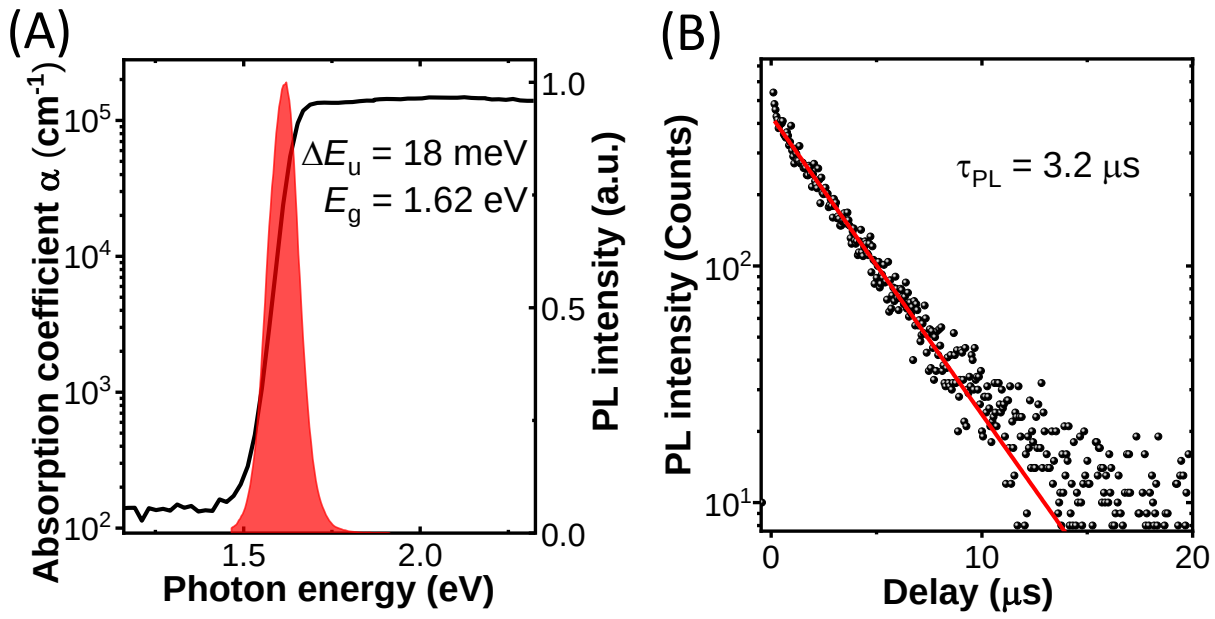

Figure 3. (A) The black solid line indicates the Photothermal Deflection Spectroscopy (PDS) measurement of the absorption coefficient as a function of the incident photon energy. The spectrum indicates a gap energy E_g = 1.62 eV and an Urbach energy ΔE_u = 18 meV. The red area represents the photoluminescence intensity measured at room temperature as a function of emitted photon energy. (B) Time resolved photoluminescence, acquired at photon energy 1.62 eV and at room temperature as a function of delay time from the photoexcitation.

The GACsFAMA absorber has been characterized by different optical techniques. Photo-thermal Deflection Spectroscopy (PDS) has been performed to measure the light absorption of the perovskite films. The PDS spectrum of Fig. 3A shows a sharp drop in absorption coefficient at the band gap value E_g = 1.62 eV (determined from photothermal deflection data by extrapolating the absorption edge). This finding is in agreement with recent reports on quadruple cation perovskites.[8,9] Below 1.5 eV, the absorption coefficient is close to 10^2 cm^{-1} while it reaches 10^5 cm^{-1} at 1.7 eV. Below gap absorption coefficient is attributed to photon absorption by shallow

tail states. The exponential rise of absorption coefficient near the bandgap results in an Urbach energy ΔE_u = 18.5 meV. For a typical $MAPbI_3$ perovskite the Urbach energy usually is 13 to 15 meV, indicating increased degree of disorder in GACsMAFA samples.[39] The steady-state photoluminescence (PL) shown in Fig. 3A peaks at the band gap (1.62 eV) and leads to a sharp emission line. Fig. 3B plots the temporal evolution of the photoluminescence intensity measured at the gap value after a photoexcitation pulse with a density of 10^{12}-10^{13} cm^{-2}. The curve can be correctly fitted by a step function multiplied with a single exponential decay function with a decay time of τ_{PL} = 3.2 µs together. The luminescence lifetime value is comparable to the relaxation time that has been previously reported for halide perovskite thin films incorporating guanidinium.[11] The remarkable increase of τ_{PL} in the presence of guanidinium confirms the efficient passivation of non-radiative recombination centers at the grain boundaries of the quadruple cation mixed halide perovskite. Overall, the suitable E_g value, high absorption coefficient, low ΔE_u, and long τ_{PL} are favorable parameters for an efficient harvesting of the solar energy.

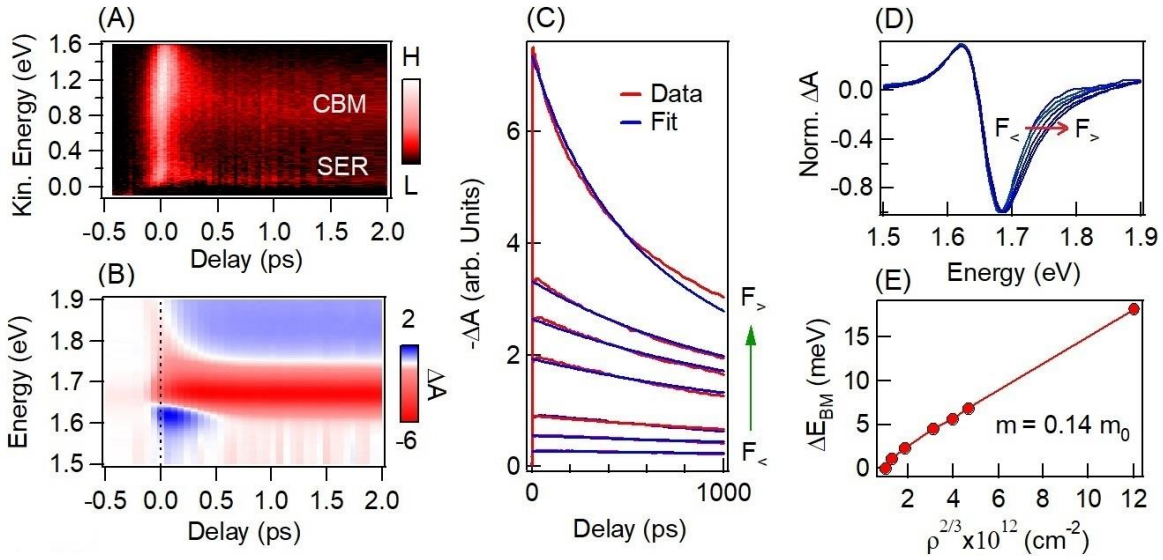

Figure 4. (A) Two photon photoemission spectroscopy (2PPE) measured on a GACsFAMA single crystal. The sample is excited with a pulse centered at 3 eV and photoelectrons are emitted by probe pulse centered at 4.5 eV. Pump on minus pump off signal of primary electrons in the Conduction Band Minimum (CBM) and Secondary Electrons Replica (SER) are marked directly on the image. (B) Differential absorption of a supercontinuum spectrum measured on a GACsFAMA thin film as a function of pump-probe delay. The pump pulse is centered at 2.5 eV and induces an excitation density of 8.7×10^{16} cm^{-3}. (C) Differential absorption decay extracted at 1.68 eV after a pump pulse centered at 2.5 eV and with different fluence values. The traces have been acquired for an excitation density spanning from 3.7×10^{16} to $7.5\times10^{17}cm^{-3}$. Red curves are the experimental data while blue curves are fits obtained via a recombination model. (D) Renormalized traces of the time-resolved transient absorption spectra acquired at pump probe delay of 0.1 ps, for increasing photoexcitation density (E) The broadening of transient absorption peak (red dots) is plot against the photoexcitation density $\rho^{2/3}$.

The initial dynamics of charge carriers after an ultrafast photoexcitation has been characterized by two different pump-probe experiments. Two-photon photoemission (2PPE) has been performed to observe the temporal evolution of the excited state in terms of kinetic energy of electrons.[40] Single crystals of GACsFAMA were cleaved and measured in ultrahigh vacuum. The entire experiment has been performed at the temperature of 180 K, in order to avoid the alteration of surface composition by possible sublimation of iodine or organic cations from the surface. The surface of the freshly cleaved crystal was photoexcited with a pump fluence of 8 $\mu J/cm^2$, centered at 3 eV and the population of photoelectrons was probed with a subsequent pulse, centered at 4.5 eV. Fig. 4A shows the pump-on minus pump off photoelectron intensity as a function of kinetic energy and pump-probe delay. The kinetic energy E_k has been referred to the vacuum level of the GACsFAMA surface but should be increased by 0.4 eV if referred to the spectrometer vacuum level. Around zero delay, primary electrons extend up to high kinetic energy and relax their excess energy until reaching the Conduction Band Minimum (CBM) at E_k = 0.8 eV. The characteristic timescale of such electronic cooling is 0.25 ps and matches the value measured[18] in $CH_3NH_3PbI_3$. Such fast relaxation of the excited electrons is ascribed to highly dissipative collisions between electrons with large excess energy and the $-NH_2$, -CH, $-NH_3^+$, $-CH_3$ groups of the organic cations.[18] This efficient carrier cooling and the negligible effect that any phonon bottleneck has at low fluence,[41] hinder any viable application of halide perovskites for the realization of hot carrier solar cells. In this context, we stress that a careful analysis of 2PPE spectra must be done to disentangle spurious components out of the measured signal. Beside the primary photoelectrons at $E_k > 0.8$ eV, an additional intensity is indeed detected for 0 eV $< E_k <$ 0.8 eV. We ascribe this Secondary Electrons Replica (SER) to photoelectrons experiencing inelastic scattering events while propagating from the sample out in the vacuum

region. The SER can be viewed as an artifact of the measurement and carries no information about the energy of excited electrons in the solid. Next, we characterized the ultrafast electron relaxation by time-resolved transient absorption at room temperature. Thin films of GACsFAMA have been probed using a white light continuum and pumped by a femtosecond pulse centered a 2.5 eV. Fig. 4B shows that Photoinduced Band Filling (PBF) reduces the absorption around 1.68 eV due to Pauli blocking.[21] In addition to this bleaching effect, a transient increase of optical absorption occurs at 1.62 eV at early delay time. The dynamical screening of the electron-electron interaction in the photoexcited state is the main reason of such Band Gap Renormalization (BGR).[19] Remarkably, the good matching between the duration of BGR in Fig. 4B and the duration of electronic cooling in Fig. 4A proves that BGR takes place while the electrons and holes are in a highly non thermal state. This result is somehow expected. Being driven by changes of dielectric function, the BGR is largest when the non-equilibrium electronic distribution opens a large amount intraband scattering channels. This condition is no longer verified after roughly 0.5 ps, once the carriers have been fully thermalized. On the longer timescale the dynamics is ruled by a reduction of PBF due to carrier recombination. We show in Fig. 4C the decay of the PBF for different excitation density between $F \leq 3.7\times10^{16}$ cm^{-3} and $F \geq 7.5\times10^{17} cm^{-3}$. The entire data set can be fit globally by standard rate equation $-\frac{dN}{dt} = aN + bN^2$ with a Shockley-Read-Hall trap recombination rate of $a = 3\times10^5$ 1/s and radiative recombination coefficient $b = 1.2\times10^{-9}$ cm^3/s (not corrected for photon recycling).[42,43] More details on the fitting procedure is given in the Supporting information. This value of radiative recombination is slightly higher compared to the radiative recombination rate reported in other halide perovskites,[44] however, as it was shown by other authors, carrier recombination rate has less effect on photovoltaic properties in materials with high carrier mobilities.[20] It is often being

wrongly argued that the high efficiency of lead-halide perovskite solar cells is due to the exceptionally slow radiative recombination rates, five orders of magnitude lower than predicted by a Langevin model.[45] The latter has been ascribed to a slightly indirect band gap originating from dynamical effects.[46] Due to thermal fluctuations, the rotation of organic cations may induce a momentum mismatch between the band edges.[47,48] Despite such proposals, recent calculations suggest that the indirect nature of the band gap suppresses the radiative recombination rate by less than a factor of two.[49] This suppression would not affect the efficiency of a perovskite solar cell as long as the carrier mobilities remain modest ($> 4\times10^{-3}$cm^2/Vs).[20] In agreement with this finding, we stress that the radiative recombination coefficient of GACsFAMA is as high as in Gallium Arsenide (GaAs), which is a traditional semiconductor with direct band gap.[50] Moreover, the long carrier lifetime observed in Fig. 2C and the high EQE in Fig. 2D imply that radiative recombination has no impact on the overall performance of the GACsFAMA solar cell. In Fig. 4D, we show the normalized transient absorption that has been measured just after photoexcitation at different pump fluence. By increasing photoexcitation density, we observe a blue shift and broadening of the PBF peak.[21,22] This dynamical Burstein-Moss effect is a consequence of the excited distribution of electron in the conduction band and holes in the valence band. It can be described by an effective filling level leading to Pauli blocking of the optical transitions in an energy interval $\Delta E_{BM} = \frac{h^2}{2m_{eh}^*}(3\pi^2 N)^{2/3}$ from the bandgap value. Here, m_{eh}^* is the reduced effective mass and N is the photoexcitation density. Fig. 4E shows the experimental broadening of PBF as a function of the excitation density to the power of 2/3. The curve is non-linear in the low fluence regime, correlated with trap filling mechanism, and linear at elevated fluence, where band-to-band recombination becomes dominant. The linear dependence observed in a wide fluence range is consistent with the simple Burstein Moss model.

From the slope of the linear fit we extract a reduced effective mass $m_{eh}^{*} = 0.14\ m_0$ (where m_0 is the bare electron mass). This value is consistent with the $0.1\ m_0 - 0.3\ m_0$[21,22] reported in $CH_3NH_3PbI_3$ or other perovskites. The relatively small value of the reduced mass, long carrier lifetime and modest diffusion rate are in good agreement with ab-initio calculations suggest a moderate dressing of GACsFAMA carriers by the lattice polarization.[23]

In conclusion, we reported a detailed chemical and time resolved spectroscopic analysis of a quadruple cation mixed halide $GA_{0.015}Cs_{0.046}MA_{0.152}FA_{0.787}Pb(I_{0.815}Br_{0.185})_3$ perovskite and comparatively analyze the micro- to femtosecond photodynamics in polycrystalline and single crystal samples. Our solar cells based on this active layer reach photovoltaic efficiencies above 20% and high operational stability. By making use of complementary ultrafast techniques, we prove that both hot carrier cooling and bandgap renormalization occur on the sub-picosecond timescale. The radiative recombination of $GA_{0.015}Cs_{0.046}MA_{0.152}FA_{0.787}Pb(I_{0.815}Br_{0.185})_3$ is higher than the one of $CH_3NH_3PbI_3$ but has no role on the photovoltaic performances of solar cells due to good carrier transport properties. On the other hand, guanidinium cations passivate the recombination centers at the grain boundaries and increases the lifetime of charge carriers drastically up to the microsecond timescale.

ASSOCIATED CONTENT

Supporting Information.

i) single crystal of quadruple cation perovskite, ii) thermogravimetric analysis of GACsMAFA and scanning electron microscopy and atomic force microscopy images of GACsMAFA thin films. iii) reference NMR data of single organic cations, iv) X-ray photoelectron spectroscopy data

AUTHOR INFORMATION

Sanjay.Mathur@uni-koeln.de

luca.perfetti@polytechnique.edu

pvl@ph2.uni-koeln.de

Notes

The authors declare no competing financial interest.

ACKNOWLEDGMENT

S.M. is thankful to the German Science Foundation (DFG) for the funding provided in the framework of the SPP Perovskites “SPP 2196/1 - Perovskite semiconductors: From fundamental properties to devices”. S.O. acknowledges the Japan Society for the Promotion of Science (JSPS) for the JSPS postdoctoral fellowship. The authors acknowledge discussion with Catherine Corbel and financial support from the ANR program TRAPPER. D.G., B.K. and T.K. thank the Initiative and Networking Fund of the Helmholtz Association for funding of the JOSEPH cluster system via the Helmholtz Energy Materials Characterization Platform (HEMCP) and for funding

via the project PEROSEED. The authors gratefully acknowledge the University of Cologne (Excellence Program “Quantum Matter and Materials”).

REFERENCES

(1) Zhang, L.; Yang, X.; Jiang, Q.; Wang, P.; Yin, Z.; Zhang, X.; Tan, H.; Yang, Y. M.; Wei, M.; Sutherland, B. R.; et al. Ultra-Bright and Highly Efficient Inorganic Based Perovskite Light-Emitting Diodes. *Nat. Commun.* **2017**, *8*, 1–8.

(2) Kojima, A.; Teshima, K.; Shirai, Y.; Miyasaka, T. Organometal Halide Perovskites as Visible-Light Sensitizers for Photovoltaic Cells. *J. Am. Chem. Soc.* **2009**, *131* (17), 6050–6051.

(3) Leyden, M. R.; Meng, L.; Jiang, Y.; Ono, L. K.; Qiu, L.; Juarez-Perez, E. J.; Qin, C.; Adachi, C.; Qi, Y. Methylammonium Lead Bromide Perovskite Light-Emitting Diodes by Chemical Vapor Deposition. *J. Phys. Chem. Lett.* **2017**, *8* (14), 3193–3198.

(4) He, Y.; Matei, L.; Jung, H. J.; McCall, K. M.; Chen, M.; Stoumpos, C. C.; Liu, Z.; Peters, J. A.; Chung, D. Y.; Wessels, B. W.; et al. High Spectral Resolution of Gamma-Rays at Room Temperature by Perovskite CsPbBr 3 Single Crystals. *Nat. Commun.* **2018**, *9* (1), 1–8.

(5) Tathavadekar, M.; Krishnamurthy, S.; Banerjee, A.; Nagane, S.; Gawli, Y.; Suryawanshi, A.; Bhat, S.; Puthusseri, D.; Mohite, A. D.; Ogale, S. Low-Dimensional Hybrid Perovskites as High Performance Anodes for Alkali-Ion Batteries. *J. Mater. Chem. A* **2017**, *5* (35), 18634–18642.

(6) Ha, S. T.; Zhang, Q.; Zhao, L.; Su, R.; Du, W.; Liu, X.; Xiong, Q. Advances in Small Perovskite-Based Lasers. *Small Methods*. **2017**, *1*, 1700163.

(7) Marco, N. De; Zhou, H.; Chen, Q.; Sun, P.; Liu, Z.; Meng, L.; Yao, E. P.; Liu, Y.; Schiffer, A.; Yang, Y. Guanidinium: A Route to Enhanced Carrier Lifetime and Open-Circuit Voltage in Hybrid Perovskite Solar Cells. *Nano Lett.* **2016**, *16* (2), 1009–1016.

(8) Wu, S.; Li, Z.; Zhang, J.; Liu, T.; Zhu, Z.; Jen, A. K. Y. Efficient Large Guanidinium Mixed Perovskite Solar Cells with Enhanced Photovoltage and Low Energy Losses. *Chem. Commun.* **2019**, *55* (30), 4315–4318.

(9) Zhang, W.; Xiong, J.; Li, J.; Daoud, W. A. Guanidinium Induced Phase Separated Perovskite Layer for Efficient and Highly Stable Solar Cells. *J. Mater. Chem. A* **2019**, *7* (16), 9486–9496.

(10) Yao, J.; Wang, H.; Wang, P.; Gurney, R. S.; Intaniwet, A.; Ruankham, P.; Choopun, S.; Liu, D.; Wang, T. Trap Passivation and Efficiency Improvement of Perovskite Solar Cells by a Guanidinium Additive. *Mater. Chem. Front.* **2019**, *3* (7), 1357–1364.

(11) Kubicki, D. J.; Prochowicz, D.; Hofstetter, A.; Saski, M.; Yadav, P.; Bi, D.; Pellet, N.; Lewiński, J.; Zakeeruddin, S. M.; Grätzel, M.; et al. Formation of Stable Mixed Guanidinium–Methylammonium Phases with Exceptionally Long Carrier Lifetimes for High-Efficiency Lead Iodide-Based Perovskite Photovoltaics. *J. Am. Chem. Soc.* **2018**, *140* (9), 3345–3351.

(12) Christians, J. A.; Schulz, P.; Tinkham, J. S.; Schloemer, T. H.; Harvey, S. P.; Tremolet de Villers, B. J.; Sellinger, A.; Berry, J. J.; Luther, J. M. Tailored Interfaces of

Unencapsulated Perovskite Solar Cells for >1,000 Hour Operational Stability. *Nat. Energy* **2018**, *3* (1), 68–74.

(13) Bai, S.; Da, P.; Li, C.; Wang, Z.; Yuan, Z.; Fu, F.; Kawecki, M.; Liu, X.; Sakai, N.; Wang, J. T.-W.; et al. Planar Perovskite Solar Cells with Long-Term Stability Using Ionic Liquid Additives. *Nature* **2019**, *571* (7764), 245–250.

(14) Pham, N. D.; Zhang, C.; Tiong, V. T.; Zhang, S.; Will, G.; Bou, A.; Bisquert, J.; Shaw, P. E.; Du, A.; Wilson, G. J.; et al. Tailoring Crystal Structure of FA 0.83 Cs 0.17 PbI 3 Perovskite Through Guanidinium Doping for Enhanced Performance and Tunable Hysteresis of Planar Perovskite Solar Cells. *Adv. Funct. Mater.* **2019**, *29* (1), 1806479.

(15) Hou, X.; Hu, Y.; Liu, H.; Mei, A.; Li, X.; Duan, M.; Zhang, G.; Rong, Y.; Han, H. Effect of Guanidinium on Mesoscopic Perovskite Solar Cells. *J. Mater. Chem. A* **2017**, *5* (1), 73–78.

(16) Jodlowski, A. D.; Roldán-Carmona, C.; Grancini, G.; Salado, M.; Ralaiarisoa, M.; Ahmad, S.; Koch, N.; Camacho, L.; De Miguel, G.; Nazeeruddin, M. K. Large Guanidinium Cation Mixed with Methylammonium in Lead Iodide Perovskites for 19% Efficient Solar Cells. *Nat. Energy* **2017**, *2* (12), 972–979.

(17) Niesner, D.; Zhu, H.; Miyata, K.; Joshi, P. P.; Evans, T. J. S.; Kudisch, B. J.; Trinh, M. T.; Marks, M.; Zhu, X.-Y. Persistent Energetic Electrons in Methylammonium Lead Iodide Perovskite Thin Films. *J. Am. Chem. Soc.* **2016**, *138* (48), 15717–15726.

(18) Chen, Z.; Lee, M. I.; Zhang, Z.; Diab, H.; Garrot, D.; Lédée, F.; Fertey, P.; Papalazarou, E.; Marsi, M.; Ponseca, C.; et al. Time-Resolved Photoemission Spectroscopy of

Electronic Cooling and Localization in CH3 NH3 PbI3 Crystals. *Phys. Rev. Mater.* **2017**, *1* (4), 1–6.

(19) Chen, K.; Barker, A. J.; Morgan, F. L. C.; Halpert, J. E.; Hodgkiss, J. M. Effect of Carrier Thermalization Dynamics on Light Emission and Amplification in Organometal Halide Perovskites. *J. Phys. Chem. Lett.* **2015**, *6* (1), 153–158.

(20) Kirchartz, T.; Krückemeier, L.; Unger, E. L. Research Update: Recombination and Open-Circuit Voltage in Lead-Halide Perovskites. *APL Mater.* **2018**, *6* (10), 100702.

(21) Manser, J. S.; Kamat, P. V. Band Filling with Free Charge Carriers in Organometal Halide Perovskites. *Nat. Photonics* **2014**, *8* (9), 737–743.

(22) Zeng, X.-H.; Cheng, L.-W.; Tanaka, K.; Yang, J.-P.; Zhang, X.-Y.; Kera, S.; Ideta, S.; Ueno, N.; Yamaguchi, T.; Ueba, T.; et al. Band Dispersion and Hole Effective Mass of Methylammonium Lead Iodide Perovskite. *Sol. RRL* **2018**, *2* (10), 1800132.

(23) Park, M.; Neukirch, A. J.; Reyes-Lillo, S. E.; Lai, M.; Ellis, S. R.; Dietze, D.; Neaton, J. B.; Yang, P.; Tretiak, S.; Mathies, R. A. Excited-State Vibrational Dynamics toward the Polaron in Methylammonium Lead Iodide Perovskite. *Nat. Commun.* **2018**, *9* (1), 2525.

(24) Liu, Y.; Yang, Z.; Cui, D.; Ren, X.; Sun, J.; Liu, X.; Zhang, J.; Wei, Q.; Fan, H.; Yu, F.; et al. Two-Inch-Sized Perovskite CH 3 NH 3 PbX 3 (X = Cl, Br, I) Crystals: Growth and Characterization. *Adv. Mater.* **2015**, *27* (35), 5176–5183.

(25) Yang, J.; Siempelkamp, B. D.; Mosconi, E.; De Angelis, F.; Kelly, T. L. Origin of the Thermal Instability in CH3NH3PbI3 Thin Films Deposited on ZnO. *Chem. Mater.* **2015**, *27* (12), 4229–4236.

(26) Han, Q.; Bae, S.-H.; Sun, P.; Hsieh, Y.-T.; Yang, Y. M.; Rim, Y. S.; Zhao, H.; Chen, Q.; Shi, W.; Li, G.; et al. Single Crystal Formamidinium Lead Iodide (FAPbI 3): Insight into the Structural, Optical, and Electrical Properties. *Adv. Mater.* **2016**, *28* (11), 2253–2258.

(27) Eperon, G. E.; Stranks, S. D.; Menelaou, C.; Johnston, M. B.; Herz, L. M.; Snaith, H. J. Formamidinium Lead Trihalide: A Broadly Tunable Perovskite for Efficient Planar Heterojunction Solar Cells. *Energy Environ. Sci.* **2014**, *7* (3), 982.

(28) Amat, A.; Mosconi, E.; Ronca, E.; Quarti, C.; Umari, P.; Nazeeruddin, M. K.; Grätzel, M.; De Angelis, F. Cation-Induced Band-Gap Tuning in Organohalide Perovskites: Interplay of Spin–Orbit Coupling and Octahedra Tilting. *Nano Lett.* **2014**, *14* (6), 3608–3616.

(29) Saliba, M.; Matsui, T.; Seo, J.-Y.; Domanski, K.; Correa-Baena, J.-P.; Nazeeruddin, M. K.; Zakeeruddin, S. M.; Tress, W.; Abate, A.; Hagfeldt, A.; et al. Cesium-Containing Triple Cation Perovskite Solar Cells: Improved Stability, Reproducibility and High Efficiency. *Energy Environ. Sci.* **2016**, *9* (6), 1989–1997.

(30) Jacobsson, T. J.; Correa-Baena, J.-P.; Halvani Anaraki, E.; Philippe, B.; Stranks, S. D.; Bouduban, M. E. F.; Tress, W.; Schenk, K.; Teuscher, J.; Moser, J.-E.; et al. Unreacted PbI 2 as a Double-Edged Sword for Enhancing the Performance of Perovskite Solar Cells. *J. Am. Chem. Soc.* **2016**, *138* (32), 10331–10343.

(31) Giordano, F.; Abate, A.; Correa Baena, J. P.; Saliba, M.; Matsui, T.; Im, S. H.; Zakeeruddin, S. M.; Nazeeruddin, M. K.; Hagfeldt, A.; Graetzel, M. Enhanced Electronic Properties in Mesoporous TiO2 via Lithium Doping for High-Efficiency Perovskite Solar Cells. *Nat. Commun.* **2016**, *7* (1), 10379.

(32) Singh, T.; Öz, S.; Sasinska, A.; Frohnhoven, R.; Mathur, S.; Miyasaka, T. Sulfate-Assisted Interfacial Engineering for High Yield and Efficiency of Triple Cation Perovskite Solar Cells with Alkali-Doped TiO 2 Electron-Transporting Layers. *Adv. Funct. Mater.* **2018**, *28* (14), 1706287.

(33) Neukom, M. T.; Züfle, S.; Knapp, E.; Makha, M.; Hany, R.; Ruhstaller, B. Why Perovskite Solar Cells with High Efficiency Show Small IV-Curve Hysteresis. *Sol. Energy Mater. Sol. Cells* **2017**, *169* (November 2016), 159–166.

(34) Zhao, Z.; Chen, X.; Wu, H.; Wu, X.; Cao, G. Probing the Photovoltage and Photocurrent in Perovskite Solar Cells with Nanoscale Resolution. *Adv. Funct. Mater.* **2016**, *26* (18), 3048–3058.

(35) Stranks, S. D.; Eperon, G. E.; Grancini, G.; Menelaou, C.; Alcocer, M. J. P.; Leijtens, T.; Herz, L. M.; Petrozza, A.; Snaith, H. J. Electron-Hole Diffusion Lengths Exceeding 1 Micrometer in an Organometal Trihalide Perovskite Absorber. *Science (80-.).* **2013**, *342* (6156), 341–344.

(36) Li, Y.; Yan, W.; Li, Y.; Wang, S.; Wang, W.; Bian, Z.; Xiao, L.; Gong, Q. Direct Observation of Long Electron-Hole Diffusion Distance in CH3NH3PbI3 Perovskite Thin Film. *Sci. Rep.* **2015**, *5* (1), 14485.

(37) De Wolf, S.; Holovsky, J.; Moon, S. J.; Löper, P.; Niesen, B.; Ledinsky, M.; Haug, F. J.; Yum, J. H.; Ballif, C. Organometallic Halide Perovskites: Sharp Optical Absorption Edge and Its Relation to Photovoltaic Performance. *J. Phys. Chem. Lett.* **2014**, *5* (6), 1035–1039.

(38) Faure, J.; Mauchain, J.; Papalazarou, E.; Yan, W.; Pinon, J.; Marsi, M.; Perfetti, L. Full Characterization and Optimization of a Femtosecond Ultraviolet Laser Source for Time and Angle-Resolved Photoemission on Solid Surfaces. *Rev. Sci. Instrum.* **2012**, *83* (4), 043109.

(39) Price, M. B.; Butkus, J.; Jellicoe, T. C.; Sadhanala, A.; Briane, A.; Halpert, J. E.; Broch, K.; Hodgkiss, J. M.; Friend, R. H.; Deschler, F. Hot-Carrier Cooling and Photoinduced Refractive Index Changes in Organic–Inorganic Lead Halide Perovskites. *Nat. Commun.* **2015**, *6* (1), 8420.

(40) Staub, F.; Hempel, H.; Hebig, J.-C.; Mock, J.; Paetzold, U. W.; Rau, U.; Unold, T.; Kirchartz, T. Beyond Bulk Lifetimes: Insights into Lead Halide Perovskite Films from Time-Resolved Photoluminescence. *Phys. Rev. Appl.* **2016**, *6* (4), 044017.

(41) Crothers, T. W.; Milot, R. L.; Patel, J. B.; Parrott, E. S.; Schlipf, J.; Müller-Buschbaum, P.; Johnston, M. B.; Herz, L. M. Photon Reabsorption Masks Intrinsic Bimolecular Charge-Carrier Recombination in CH3NH3PbI3 Perovskite. *Nano Lett.* **2017**, *17* (9), 5782–5789.

(42) Kirchartz, T. High Open-Circuit Voltages in Lead-Halide Perovskite Solar Cells: Experiment, Theory and Open Questions. *Philos. Trans. R. Soc. A Math. Phys. Eng. Sci.* **2019**, *377* (2152), 20180286.

(43) Wehrenfennig, C.; Liu, M.; Snaith, H. J.; Johnston, M. B.; Herz, L. M. Charge-Carrier Dynamics in Vapour-Deposited Films of the Organolead Halide Perovskite CH3NH3PbI3-XClx. *Energy Environ. Sci.* **2014**, *7* (7), 2269–2275.

(44) Liu, S.; Zheng, F.; Koocher, N. Z.; Takenaka, H.; Wang, F.; Rappe, A. M. Ferroelectric Domain Wall Induced Band Gap Reduction and Charge Separation in Organometal Halide Perovskites. *J. Phys. Chem. Lett.* **2015**, *6* (4), 693–699.

(45) Zheng, F.; Tan, L. Z.; Liu, S.; Rappe, A. M. Rashba Spin–Orbit Coupling Enhanced Carrier Lifetime in CH 3 NH 3 PbI 3. *Nano Lett.* **2015**, *15* (12), 7794–7800.

(46) Niesner, D.; Wilhelm, M.; Levchuk, I.; Osvet, A.; Shrestha, S.; Batentschuk, M.; Brabec, C.; Fauster, T. Giant Rashba Splitting in CH3NH3 Organic-Inorganic Perovskite. *Phys. Rev. Lett.* **2016**, *117* (12), 126401.

(47) Zhang, X.; Shen, J.-X.; Wang, W.; Van de Walle, C. G. First-Principles Analysis of Radiative Recombination in Lead-Halide Perovskites. *ACS Energy Lett.* **2018**, *3* (10), 2329–2334.

(48) 'T Hooft, G. W. The Radiative Recombination Coefficient of GaAs from Laser Delay Measurements and Effective Nonradiative Carrier Lifetimes. *Appl. Phys. Lett.* **1981**, *39* (5), 389–390.